

# Facile Glycothermal Synthesis of $K_xNa_{(1-x)}NbO_3$ Particles

Hong-Chan Cho <sup>1</sup>, Dae-Young Lim <sup>2</sup> and Jeong-Hwan Song <sup>2,\*</sup> 

<sup>1</sup> Department of Materials Engineering, Graduate School of PaiChai University, Daejeon 35345, Korea; sc31047@nate.com

<sup>2</sup> Department of Materials Science and Engineering, PaiChai University, Daejeon 35345, Korea; dylim@pcu.ac.kr

\* Correspondence: song\_jeonghwan@pcu.ac.kr; Tel.: +82-42-520-5916; Fax: +82-70-4850-8458

**Abstract:**  $K_xNa_{(1-x)}NbO_3$  particles (KNN,  $0 < x < 1$ ) were successfully synthesized through a facile glycothermal method by using KOH, NaOH and  $Nb_2O_5$  as precursors and 1,4-butanediol as solvent at 200 °C for 12 h. The effects of varying the 1,4-butanediol/deionized water (B/W) volume ratio as solvent on the growth behavior, the morphological evolution, and the particle size of the synthesized KNN particles were investigated. In order to obtain  $K_{0.5}Na_{0.5}NbO_3$  with the morphotropic phase boundary (MPB) at the potassium content of  $x \approx 0.5$ , the effect of varying  $K^+/Na^+$  molar ratio on the composition of the obtained KNN particles was investigated. The crystal phase structure, morphology, particle size, chemical composition, and thermal behavior of the obtained particle samples were characterized using XRD, FE-SEM, EDS, TG, FT-IR, PSA, and TEM. The pure orthorhombic KNN particle close to  $NaNbO_3$  phase was obtained at the same concentration  $K^+/Na^+$  of 1.0/1.0 and  $[K^++Na^+]/Nb$  molar ratio of 2.0/0.1. The synthesized  $K_{0.01}Na_{0.99}NbO_3$  particle exhibited a hexahedron shape with an average crystallite size of approximately 400 nm by glycothermal treated at 200 °C for 12 h. It is also demonstrated that the size of Na-rich KNN particles was decreased from 15  $\mu m$  to 400 nm with increasing 1,4-butanediol content at various reaction conditions such as the volume ratio of B/W and can be controlled by 1,4-butanediol with an additive of water. Until the molar ratio of  $K^+/Na^+$  reaches 1.6/0.4, the obtained particles have produced a Na-rich KNN phase, whereas when the molar ratio of  $K^+/Na^+$  is 1.8/0.2, the particles could obtain a K-rich KNN phase. The results revealed that single-phase  $K_{0.5}Na_{0.5}NbO_3$  particles could be obtained at a relatively narrow molar ratio of  $K^+/Na^+$  to 1.7/0.3. The particles with weakened agglomerate could obtain the average particle size of approximately 400 nm and a hexahedron shape. In comparison with the traditional hydrothermal method, the glycothermal method has been confirmed to be a more efficient method in controlling the particle size of KNN particles from micro- to sub-micron.

**Keywords:**  $K_xNa_{(1-x)}NbO_3$  particle; glycothermal method; 1,4-butanediol/deionized water volume ratio;  $K^+/Na^+$  molar ratio; MPB



**Citation:** Cho, H.-C.; Lim, D.-Y.; Song, J.-H. Facile Glycothermal Synthesis of  $K_xNa_{(1-x)}NbO_3$  Particles. *Crystals* **2022**, *12*, 827. <https://doi.org/10.3390/cryst12060827>

Academic Editor: Zhi Lin

Received: 29 March 2022

Accepted: 9 June 2022

Published: 10 June 2022

**Publisher's Note:** MDPI stays neutral with regard to jurisdictional claims in published maps and institutional affiliations.



**Copyright:** © 2022 by the authors. Licensee MDPI, Basel, Switzerland. This article is an open access article distributed under the terms and conditions of the Creative Commons Attribution (CC BY) license (<https://creativecommons.org/licenses/by/4.0/>).

## 1. Introduction

Lead-containing piezoelectric ceramics, represented by  $Pb(Zr,Ti)O_3$  ceramics and  $Pb(Zr,Ti)O_3$ -based multi-component ceramics, have been widely used as actuators, transducer, and sensor materials [1–5]. However, the use of lead-containing ceramics has caused serious environmental problems because of the high toxicity of lead oxide [1,5]. Therefore, it is necessary to develop lead-free ceramics with excellent piezoelectric properties to replace such lead-based ceramics.

Research on lead-free piezoelectric materials has mainly been focused on the following material systems: tungsten bronze-type materials, bi-layer structured materials, and perovskite-type materials [6,7]. Potassium sodium niobate is considered as one of the most promising candidates for lead-free piezoelectric ceramics because of its strong piezoelectricity, ferroelectricity and high Curie temperature [8–14].  $K_xNa_{(1-x)}NbO_3$  (KNN,  $0 < x < 1$ ) is a combination of ferroelectric  $KNbO_3$  and antiferroelectric  $NaNbO_3$  [15,16], and this ceramic

forms a morphotropic phase boundary (MPB) at approximately  $x \approx 0.5$ . It is believed that in these systems, a high piezoelectric response is related to the MPB [9,10,12–18].

Although KNN is a promising piezoelectric material, there are some aspects that still need attention, in which high densities (>90% theoretical density) are difficult to attain during normal sintering, and  $K_2O$  and  $Na_2O$  easily evaporate at high temperatures often leading to potassium- and sodium-deficient phase in the composition of the final product [16,19–21]. There has been growing interest in the synthesis of KNN particles with the desired shape and size.

Recently, various approaches to the synthesis of KNN piezoelectric materials have been attempted, including solid-state reaction [9,13,22,23], spark plasma sintering [24], microwave heating method [25], molten-salt process [20], the Pechini method [21], the sol-gel method [26–28], and the hydrothermal method [10,17,29–34].

Among them, hydrothermal synthesis is currently considered a promising way to obtain high-quality ceramic particles. Compared to other solution processing techniques, the hydrothermal method has many advantages: (1) A crystalline product can be obtained directly at a lower reaction temperature, and it favors a decrease in an agglomeration between particles. (2) Crystalline products with various compositions, structures, and morphologies can be formed by changing hydrothermal conditions (such as temperature, pH, reactant concentration and molar ratio, additive, etc.) and at higher purity owing to recrystallization in hydrothermal solution. (3) The equipment and procedures required are simpler, and the control of reaction conditions is easier.

To synthesize crystalline particles using the glycothermal concepts embodied in hydrothermal processing approaches, a few investigations have studied the use of non-aqueous systems as glycol media. We have shown that a glycothermal process provides a facile low-temperature route to produce  $BaTiO_3$ ,  $Fe_3O_4$ , Y-doped  $ZrO_2$ ,  $TiO_2$ ,  $ZnO$ , and  $ZnS$  particles with the desired morphology and size, as described in our previous study [35–41]. Our research embodies some novelty concepts that differ from the reported technology for particle synthesis. First, a glycothermal process could remarkably reduce the reaction temperature and pressure for large-scale production. Second, it is facile to control the size and morphology of the synthesized particles in glycol solvent without growth agents. Therefore, this glycothermal process provides a new prospective approach for controlling the size and morphology of electronic material particles at low temperatures.

The purpose of the present work was to investigate the possibility of directly preparing KNN particles using a facile glycothermal process, adjusting conditions such as reaction temperature and reaction time. We report here the effect of 1,4-butanediol/deionized water (B/W) volume ratio on the size and morphology of KNN particles by glycothermal processes. We have investigated the effect of the various molar ratios of  $K^+/Na^+$  on the KNN synthesis. In addition, the  $K_{0.5}Na_{0.5}NbO_3$  particle with MPB composition was prepared by a glycothermal process, and the preparation conditions were studied.

## 2. Experimental Procedure

### 2.1. Glycothermal Synthesis

All experiments were conducted using  $Nb_2O_5$  (99.9%, Treibacher Industrie AG, Althofen, Austria),  $KOH$  (95%, DC Chemical, Seoul, Korea), and  $NaOH$  (98%, DC Chemical, Seoul, Korea) as the starting materials to synthesize KNN particles. Glycothermal synthesis was carried out with a mixture solvent of 1,4-butanediol (99%,  $C_4H_{10}O_2$ , Sigma-Aldrich Chemical, St. Louis, MO, USA) and deionized water. Several modifications to the standard synthesis procedure such as reaction temperature, reaction time, mixture solvent volume ratio, and  $K/Na/Nb$  molar ratio were incorporated to study the influence of different synthetic conditions on the phase, size, and morphology of the resulting particle. Anhydrous  $Nb_2O_5$  is the most common niobium source for the KNN synthesis.  $Nb_2O_5$  as the niobium source was dissolved in strong base solutions such as  $KOH$  and  $NaOH$  because it poses several problems including low solubility and low reactivity in water at room temperature [42].

First, KOH and NaOH with a  $K^+/(K^+ + Na^+)$  molar ratio equal to 0.5 were dissolved in 70 mL of 1,4-butanediol through vigorous stirring, forming a mixed alkaline solution with a total alkalinity content of 2 M. Then, the oxide powder of  $Nb_2O_5$  (0.1 M) was added to the prepared alkali solution, and after being stirred for 30 min, the resulting suspension was transferred into a 100 mL Teflon container with a filling factor of 70 vol.% for reaction in the sealed stainless-steel pressure autoclave. To determine the optimum glycothermal synthesis condition of KNN particles, reactions were carried out under different desired temperatures (80, 120, 160, and 200 °C) with a rate of 2 °C/min for various holding times (1 h, 3 h, 6 h, and 12 h).

Total solvent volume was 70 mL. The effect of solvent volume ratio on the phase and size of KNN particles was investigated by varying the content of the solvent mixtures with 1,4-butanediol and deionized water from 70/0 to 0/70 under the optimum synthesis condition at 200 °C for 12 h. KNN particles with different  $x$  values were synthesized by varying the molarity ratios of  $K^+/Na^+$  in the basic solution from 1.0/1.0 to 1.8/0.2 using glycothermal synthesis at 200 °C for 12 h. The synthesis condition of  $K_{0.5}Na_{0.5}NbO_3$  in MPB composition on KNN was determined.

After glycothermal reaction, the autoclave was cooled to room temperature. The precipitates with a light ivory color were formed on the bottom of the Teflon container. The synthesized particles were centrifuged 3 times at 8000 rpm for 15 min using deionized water to separate and wash off the reaction solvent until the pH value was equal to 7, and then washed in ethanol 2 times. After drying at 100 °C for 24 h in a dry oven, the final KNN particle was obtained.

## 2.2. Characterization

The dried, recovered particles were analyzed using X-Ray Diffraction (XRD, Smart-Lab, Rigaku,  $CuK\alpha_1$ , 45 kV/40 mA) over the  $2\theta$  range from 10° to 80° at a scan speed of 2°/min to determine the phase composition and crystal structure. Experimental data from XRD patterns were compared to standards recommended by the Joint Committee on Powder Diffraction and Standards (JCPDS) to determine the chemical identity of the products. The morphology and size of the synthesized particles were investigated using field emission-scanning electron microscopy (FE-SEM, S-4800, Hitachi, Tokyo, Japan). The composition was investigated using energy-dispersive X-ray spectroscopy (EDS, JSM-6380LA, JEOL, Tokyo, Japan). The mean particle size and size distribution of the particles were characterized using a particle size analyzer (ELS-8000, Otsuka Electronics, Osaka, Japan). Thermogravimetric analysis (TGA) was carried out to understand the decomposition and mass change of a sample, and to optimize the calcination temperature. Thermogravimetric analysis (TGA 2000, MAC Science, Yokohama, Japan) was performed under ambient air with a heating rate of 2 °C/min up to 1000 °C. Infrared absorption was measured by a Fourier transform infrared (FT-IR) spectrophotometer (FTS 300, Bio-Rad, Hercules, CA, USA) for analysis of surface impurities on the particles, such as C–O and O–H groups and carbonates using the KBr pellet technique. IR samples were prepared by mixing dry particle with dry KBr in a 1:100 ratio by weight. Transmission electron microscope (TEM, JEM-2100F, JEOL, Tokyo, Japan) was used to observe the dispersibility and crystal shape of the synthesized particles. High resolution lattice images and electron diffraction patterns also were taken to confirm the crystallinity of the internal microstructure.

## 3. Results and Discussion

### 3.1. Glycothermal Synthesis of KNN Particles

To investigate the effect of the reaction temperature on the synthesis of KNN particles, suspensions with molar ratio of K/Na/Nb to 1.0/1.0/0.1 were glycothermally treated at different temperatures. Figure 1 presents XRD patterns of each particle obtained at various reaction temperatures for the same reaction time of 12 h by glycothermal process using pure 1,4-butanediol solvent. At temperatures below 120 °C, KNN could not be formed as the reaction temperature was too low, and most peaks of  $Nb_2O_5$  with the orthorhombic

structure as the starting material were retained (JCPDS card 30-0873).  $\text{Nb}_2\text{O}_5$  content was gradually decreased as the reaction temperature increased. While the main peaks in the XRD patterns obtained at reaction temperature of 160 °C as shown in Figure 1c are those for the KNN phase, it was ascertained that the small peak still existed from the unconverted  $\text{Nb}_2\text{O}_5$  of the raw material. Phase pure KNN particles were prepared without any impurities at a reaction temperature of 200 °C. All the diffraction peaks were attributed to KNN with an orthorhombic structure, and the entire pattern matches the reference peaks reported on  $\text{NaNbO}_3$  phase (JCPDS card 73-0803). The lattice constants calculated from the XRD pattern in Figure 1d were  $a = 0.5539$  nm,  $b = 0.5576$  nm, and  $c = 1.5595$  nm.

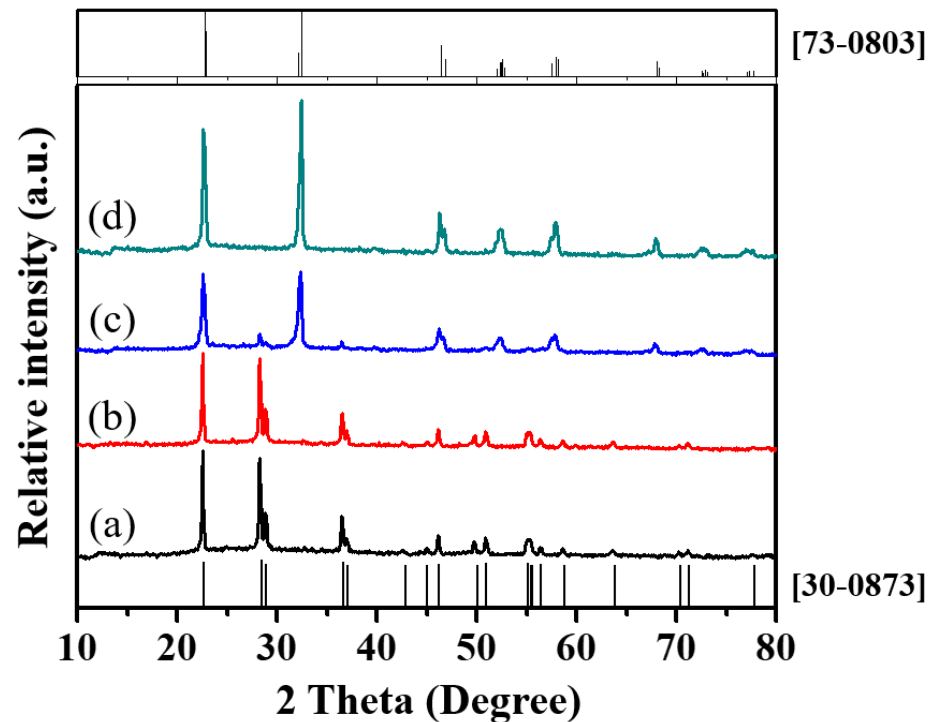


**Figure 1.** XRD patterns of KNN particles synthesized in glycothermal conditions at various reaction temperatures for 12 h: (a) 80 °C, (b) 120 °C, (c) 160 °C, and (d) 200 °C. JCPDS database for  $\text{Nb}_2\text{O}_5$  (JCPDS card 30-0873) and  $\text{NaNbO}_3$  (JCPDS card 73-0803) are also included in the figure.

The FE-SEM photomicrographs of each particle obtained at various reaction temperatures are given in Figure 2. This result shows that the particles obtained at different temperatures were formed from  $\text{Nb}_2\text{O}_5$  to KNN without the size change of precursor. The particle morphology changed from irregular polyhedral shapes to hexahedron shapes.

The diffraction patterns of the particles synthesized by the glycothermal process at 200 °C for various reaction times are presented in Figure 3a. After a reaction time of 1 h, KNN was observed with some peak of the unreacted  $\text{Nb}_2\text{O}_5$ . Although the unreacted  $\text{Nb}_2\text{O}_5$  still coexists in the reaction product until the reaction time reaches 6 h, it gradually disappeared with the increasing reaction time. Phase pure KNN particles were prepared without any impurities at a reaction time of 12 h. The diffraction peaks of KNN became sharper and stronger with increasing reaction time. Figure 3b shows the EDS analysis results for KNN particles obtained at the glycothermal condition with a molar ratio of  $\text{K}^+/\text{Na}^+$  to 1.0/1.0 at 200 °C for 12 h. The particle obtained in this condition was almost not detected in  $\text{K}^+$  content of 1 mol.%. It was found to produce  $\text{K}_{0.01}\text{Na}_{0.99}\text{NbO}_3$  particle of potassium deficient. The EDS analyses were consistent with the XRD results.

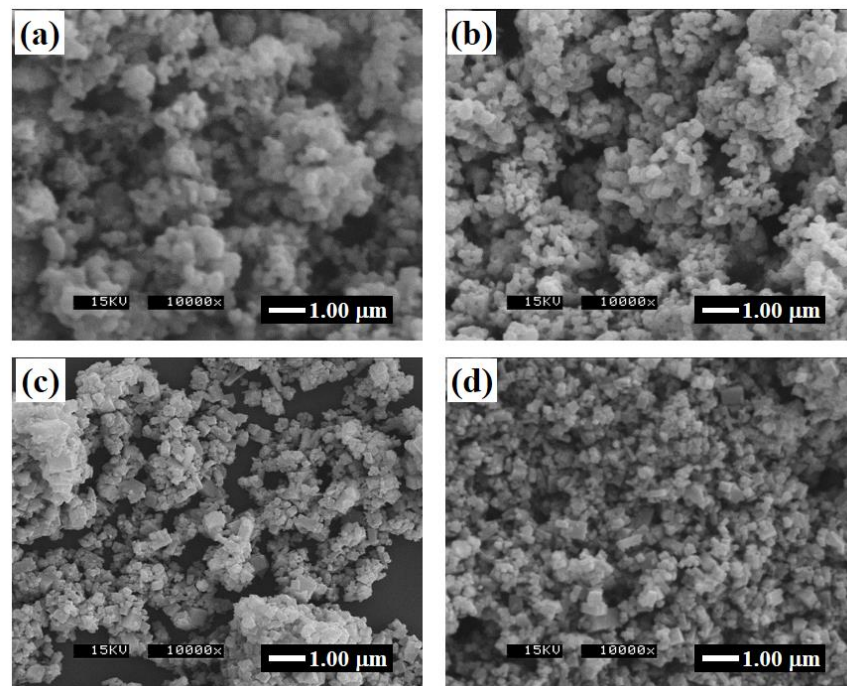


**Figure 2.** FE-SEM photomicrographs of KNN particles synthesized in glycothermal conditions at various reaction temperatures for 12 h: (a) 80 °C, (b) 120 °C, (c) 160 °C, and (d) 200 °C.

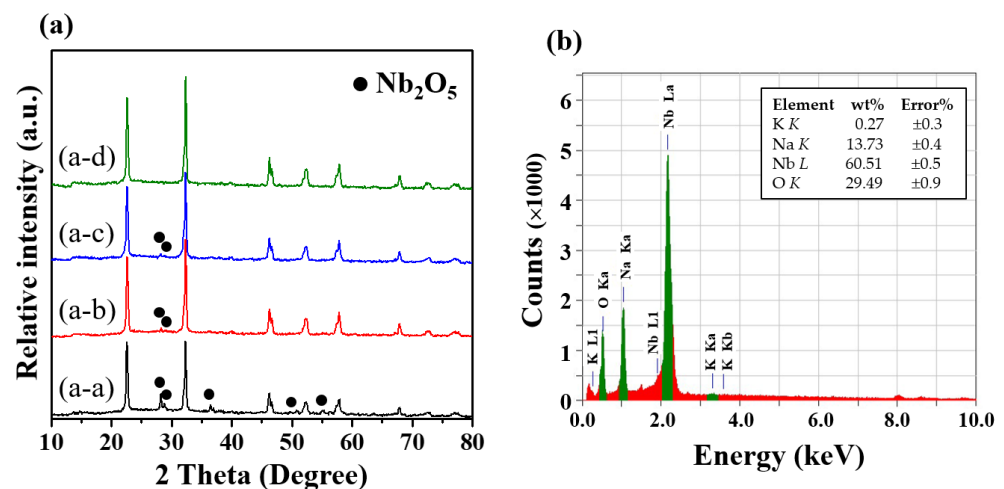


**Figure 3.** (a) XRD patterns of KNN particles synthesized in glycothermal conditions at 200 °C with various reaction times. (a-a) 1 h, (a-b) 3 h, (a-c) 6 h, and (a-d) 12 h. JCPDS database for  $\text{Nb}_2\text{O}_5$  (JCPDS card 30-0873) and  $\text{NaNbO}_3$  (JCPDS card 73-0803) are also included in the figure. (b) EDS analysis of KNN particles synthesized at 200 °C for 12 h.

In addition, the particle size and morphology of KNN particles were not dependent on reaction times. The particle sizes and morphologies of all the particles obtained appeared to show a similar tendency. This can easily be seen in the FE-SEM images, as shown in Figure 4. The obtained particles of hexahedron shapes are well dispersed with a relatively narrow particle size distribution under glycothermal conditions. It is considered that KNN was synthesized owing to the increasing solubility of  $\text{Nb}_2\text{O}_5$  in the 1,4-butanediol solvent in which a strong base component was present with the increase in reaction temperature and time. Therefore, the optimum condition for KNN particles with pure perovskite-type phase via glycothermal treatment can be achieved at 200 °C for 12 h from the perspective of the synthesis process.

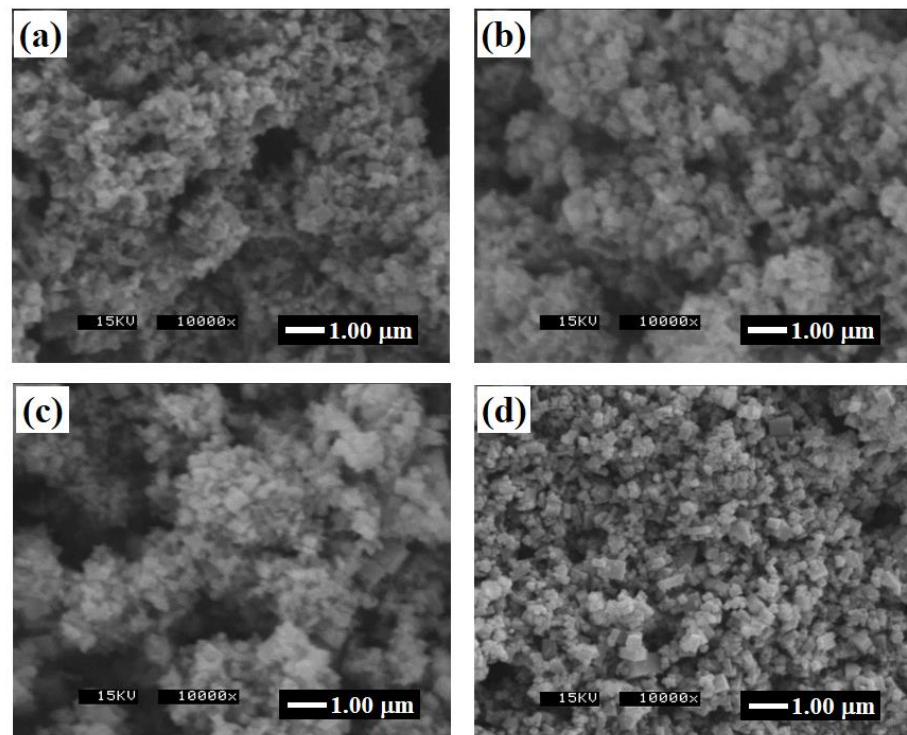


**Figure 4.** FE-SEM photomicrographs of KNN particles synthesized in glycothermal conditions at 200 °C with various reaction times: (a) 1 h, (b) 3 h, (c) 6 h, and (d) 12 h.

The effect of volume ratio of 1,4-butanediol and deionized water as solvent on the formation and particle size of KNN were investigated under synthesis condition with a molar ratio of K/Na/Nb to 1.0/1.0/0.1 at 200 °C for 12 h. Figure 5 shows the XRD patterns of KNN particles synthesized with varying B/W volume ratio from 70/0 to 0/70. As a result, all XRD patterns of the synthesized particles exhibited the perovskite structure with orthorhombic symmetry of KNN, regardless of the B/W volume ratio and confirmed that it is corresponding with  $\text{NaNbO}_3$  (JCPDS card 73-0803). No characteristic peak of any secondary phase and residues could be observed in the KNN particles, which indicates that the synthesized particles have a high crystal phase purity. The crystallite size of the KNN particle was calculated from the broadening of the main peak using Scherrer's equation:

$$D = \frac{0.94 \lambda}{\beta \cos \theta} \quad (1)$$

where  $D$  is the average crystallite size,  $\lambda$  (0.15406 nm) is the wavelength of Cu,  $\beta$  is the full-width at half-maximum, and  $\theta$  is the diffraction angle of the center of the peak. The average crystallite sizes of the synthesized KNN particle by the increasing volume ratio of deionized water were increased to approximately 40–55 nm. Careful observation revealed a peak shift in the XRD patterns in the  $2\theta$  range of from 31.5° to 33.0° as shown in Figure 5. According to the Bragg diffraction equation of  $2d\sin\theta = n\lambda$ , when  $\theta$  decreases,  $d$  value indicating the distance between the crystal planes will increase. With the higher deionized water content in the B/W volume ratio, the peaks for the particles shifted slightly to the lower angles. The values of lattice parameter are shown in Table 1.

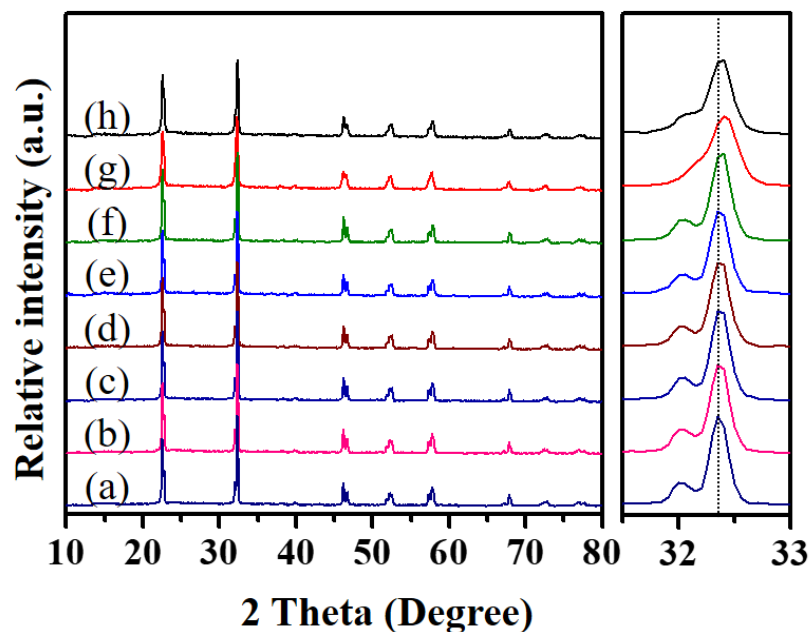


**Figure 5.** XRD patterns of KNN particles synthesized by glycothermal treatment with various solvent volume ratios of B/W at 200 °C for 12 h: (a) 0/70 (pure hydrothermal), (b) 10/60, (c) 20/50, (d) 30/40, (e) 40/30, (f) 50/20, (g) 60/10, and (h) 70/0 (pure glycothermal).

**Table 1.** The lattice parameters of KNN particles synthesized by glycothermal treatment with various solvent volume ratios of B/W at 200 °C for 12 h.

Solvent Volume Ratio (B/W)	Lattice Parameters		
	a (nm)	b (nm)	c (nm)
0/70	0.5551	0.5588	1.5589
10/60	0.5546	0.5588	1.5589
20/50	0.5543	0.5586	1.5582
30/40	0.5545	0.5584	1.5582
40/30	0.5545	0.5584	1.5582
50/20	0.5543	0.5581	1.5589
60/10	0.5532	0.5582	1.5595
70/0	0.5539	0.5576	1.5595

The size of KNN particles was strongly dependent on B/W volume ratio. From the FE-SEM photomicrographs, it can easily be seen that the size of KNN particles increased dramatically from approximately 400 nm to 15  $\mu$ m when B/W volume ratio was changed from 70/0 to 0/70 as shown in Figure 6. However, the morphology of the KNN particles remained almost unchanged with hexahedron shapes, regardless of the water content in the B/W volume ratio. This behavior can be explained by considering the solubility change in glycothermal condition using a mixed solvents containing water.

The actions of a solvent may impact crystal growth and crystallization due to the effect of the related properties on density, viscosity, solubility, diffusivity, and other factors such as heat and mass transport [43,44]. The size, phase, and morphology of the prepared crystalline particles can be significantly influenced by the chemical properties of 1,4-butanediol and water used as a solvent. Organic solvents have lower dielectric constants which result in lower solubility of inorganic material in the solution. Therefore, it is suitable to suppose that the solubility of Nb<sub>2</sub>O<sub>5</sub> in a 1,4-butanediol solvent is an essential difference compared to that in water. In general, the synthesis systems on the materials with low solubility appear with in situ transition by dehydration reaction from poorly soluble materials to crystalline agglomerates composed of nano-size primary particles. This solubility of Nb<sub>2</sub>O<sub>5</sub>

in the solution with a basic solute dissolved in 1,4-butanediol could only promote the nucleation action attributed to the short mean-free path of the solute by limiting the transport of the solute into the solid–liquid interface for crystal growth. Therefore, KNN particles of approximately 400 nm can be synthesized by a glycothermal process. In contrast, it is reasonably considered the solubility of  $\text{Nb}_2\text{O}_5$  was increased by increasing the water content in mixed glycothermal condition. The relatively high solubility of  $\text{Nb}_2\text{O}_5$  in the basic aqueous solution could support further crystal growth due to promoting the transport of the solute into the solid–liquid interface. The size of KNN particles was increased by increasing the water volume ratio.

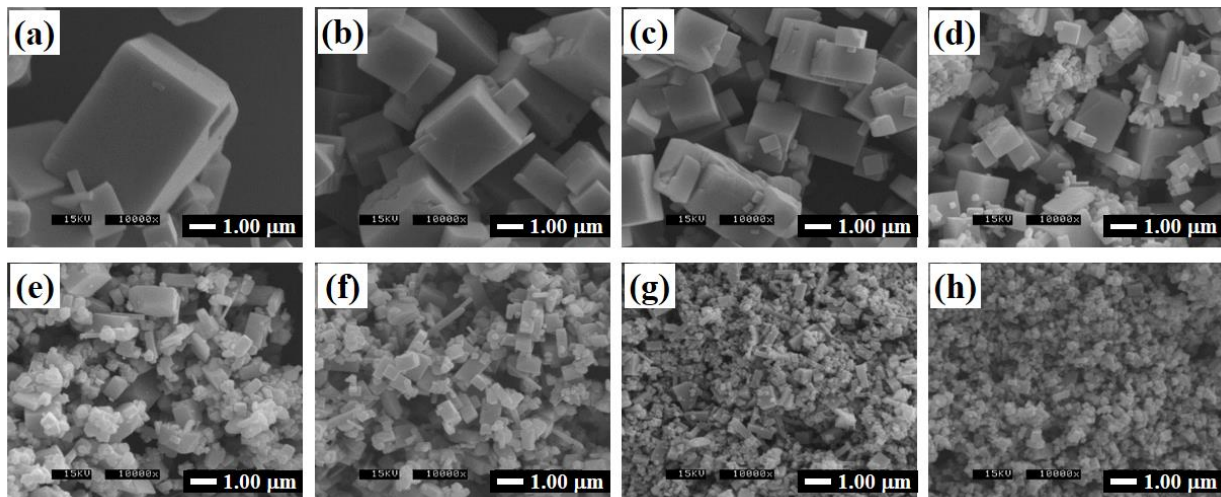


**Figure 6.** FE-SEM photomicrographs of KNN particles synthesized by glycothermal treatment with various solvent volume ratios of B/W at 200 °C for 12 h: (a) 0/70 (pure hydrothermal), (b) 10/60, (c) 20/50, (d) 30/40, (e) 40/30, (f) 50/20, (g) 60/10, and (h) 70/0 (pure glycothermal).

In addition, the particle size distributions of KNN particles synthesized with varying B/W volume ratio from 70/0 to 20/50 are shown in Figure 7. The equivalent volume diameter of the KNN particles decreased from 13  $\mu\text{m}$  to 450 nm while the B/W volume ratio was varied from 20/50 to 70/0, respectively. In a pure glycothermal condition, it is believed that  $\text{Nb}_2\text{O}_5$  was in situ transformed into KNN without the size and morphological change between the raw material and final product. In contrast, the size of KNN particles increased dramatically, which was attributed to the increased solubility of  $\text{Nb}_2\text{O}_5$  in mixed glycothermal condition with the water added. Since the equivalent volume diameter of glycothermally prepared KNN particles determined by the particle size analyzer was close to the size determined by SEM images, it appears that chemisorption of 1,4-butanediol at the surfaces of the KNN particles minimizes the aggregation of the particles by hydrogen bonding. 1,4-Butanediol at the surface of KNN particles acts as a dispersant in solvent, leading to a well-dispersed suspension without any further dispersant. Therefore, the size of KNN particles increased as a function of water content in B/W volume ratio, which can be explained by a recrystallization reaction mechanism.

Figure 8 shows TG analysis results of KNN particles synthesized by pure hydrothermal and pure glycothermal processes. Total weight losses of the particles synthesized by pure hydrothermal and pure glycothermal processes were very small at 0.6 wt.% and 2.5 wt.%, respectively. The total weight loss consists of four contributions: the first region (<200 °C) corresponds to the loss of physically adsorbed water and 1,4-butanediol, the second regions between 200 °C and 570 °C corresponds to the loss of chemically bound hydroxyl groups [36]. In the third regions between 570 °C and 670 °C, the weight loss is attributed to the combustion of carbonized species by 1,4-butanediol chemically bounded inside KNN particles and on the surface [36]. Finally, the weight loss above 670 °C is due to  $\text{CO}_2$  release from decomposition of carbonate species.

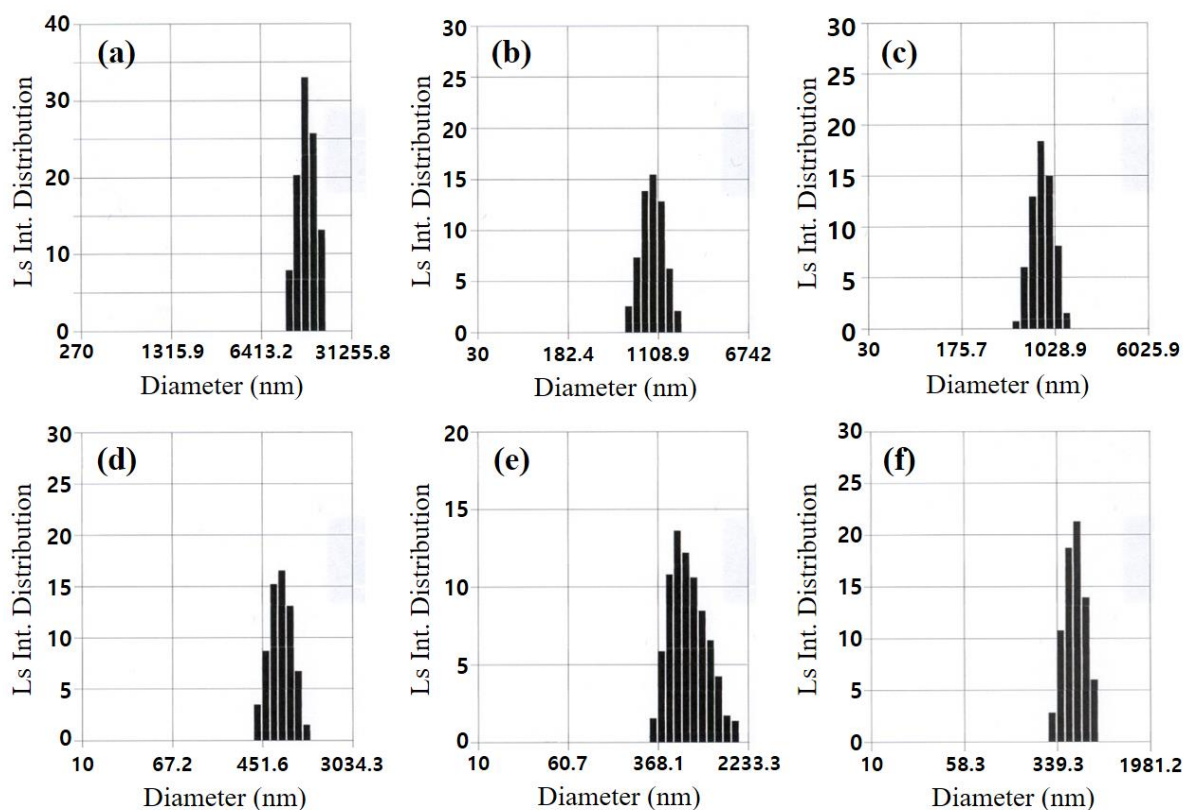


**Figure 7.** Particle size distribution of KNN particles synthesized by glycothermal treatment with various solvent volume ratios of B/W at 200 °C for 12 h: (a) 20/50, (b) 30/40, (c) 40/30, (d) 50/20, (e) 60/10, and (f) 70/0 (pure glycothermal).

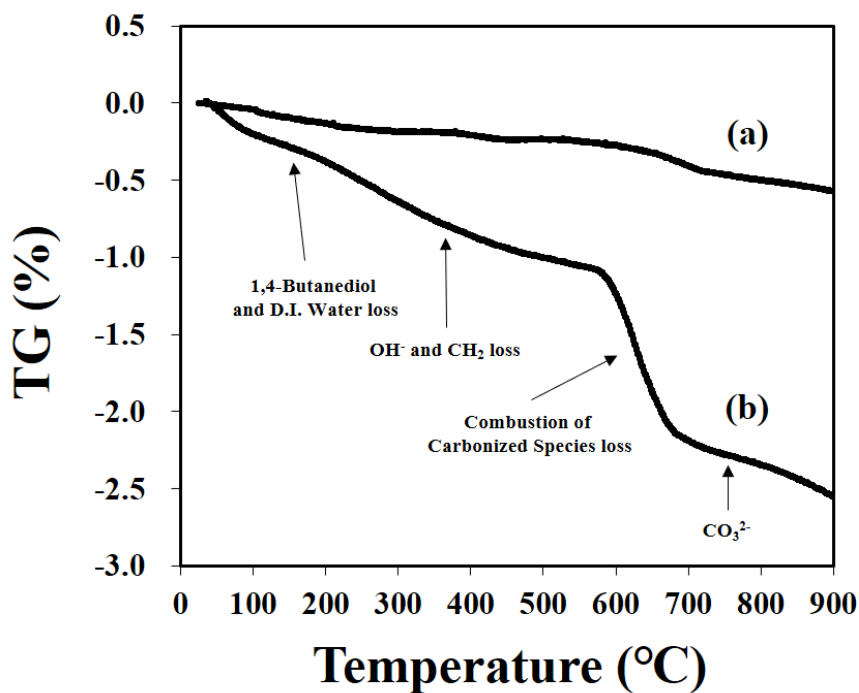


**Figure 8.** TG analysis of KNN particles synthesized by glycothermal treatment in different synthesis conditions: (a) pure hydrothermal and (b) pure glycothermal at 200 °C for 12 h.

This result was consistent with the FT-IR analyses, as shown in Figure 9. The weak band at  $1640\text{ cm}^{-1}$ , between  $3600\text{ cm}^{-1}$  and  $4000\text{ cm}^{-1}$  (bending mode of  $\text{H}_2\text{O}$ ), indicates that some  $\text{H}_2\text{O}$  is present [38,39]. The two broad peaks at around  $750\text{ cm}^{-1}$  and  $3350\text{ cm}^{-1}$  are associated with the O–H stretching vibration of absorbed water and hydroxyl group [27,38,39]. In addition, the sharp peak at  $1380\text{ cm}^{-1}$  is due to the characteristics of the  $\text{CO}_3^{2-}$  group [27,38,39]. The absorption peaks at  $1450\text{ cm}^{-1}$  and  $1560\text{ cm}^{-1}$  are due to the symmetric stretching of  $\text{CH}_2$  group, and chemisorption of 1,4-butanediol is believed to be involved in the formation of these peaks through substitution on a surface hydroxyl group [38,39].

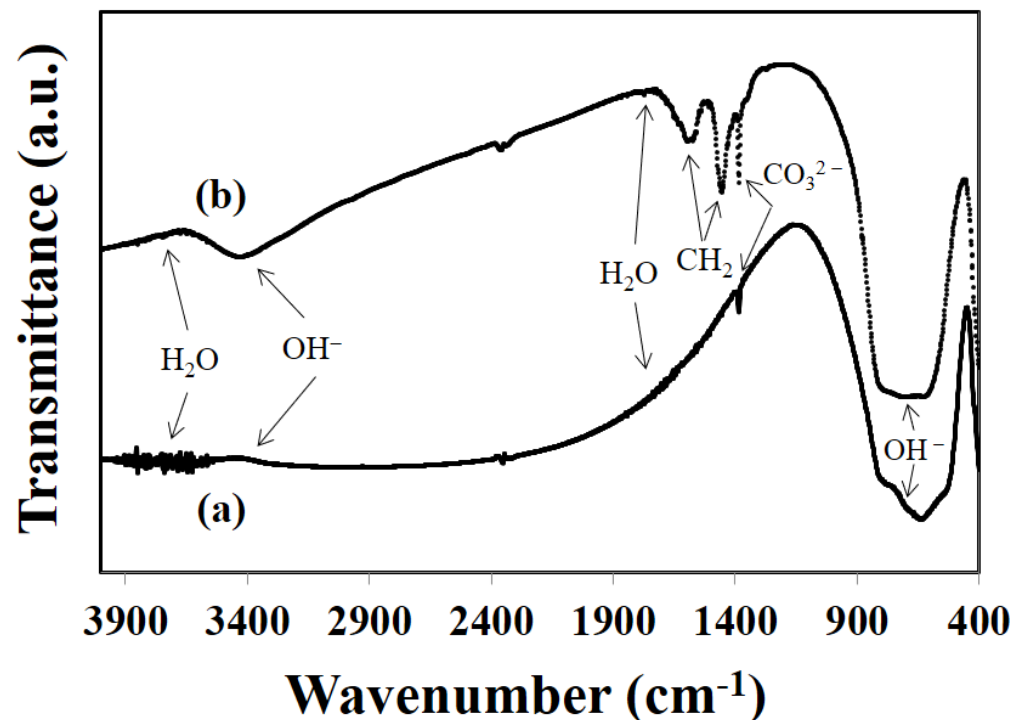


**Figure 9.** FT-IR spectra of KNN particles synthesized by glycothermal treatment in different synthesis conditions: (a) pure hydrothermal and (b) pure glycothermal at  $200\text{ }^{\circ}\text{C}$  for 12 h.

### 3.2. Glycothermal Synthesis of $\text{K}_{0.5}\text{Na}_{0.5}\text{NbO}_3$ Particles at the MPB Composition

In the case of KNN particles appear in the morphotropic phase boundary (MPB) at a potassium content of  $x \approx 0.5$ . We worked to find the experimentally optimized condition of  $\text{K}^+/\text{Na}^+$  molar ratio for the synthesis of  $\text{K}_{0.5}\text{Na}_{0.5}\text{NbO}_3$ . The varying molar ratios of  $\text{K}^+/\text{Na}^+$  in the fixed amount of  $\text{Nb}_2\text{O}_5$  (0.1 M) were glycothermally treated using only 1,4-butanediol at  $200\text{ }^{\circ}\text{C}$  for 12 h. XRD patterns of KNN particles synthesized at different molar ratios of  $\text{K}^+/\text{Na}^+$  appear in Figure 10. We can see that the patterns of KNN particles slowly shifted to the lower  $2\theta$  angles, as the molar ratio of  $\text{K}^+/\text{Na}^+$  in each solution is gradually enhanced. Because the radius of  $\text{K}^+$  (0.133 nm) is larger than that of  $\text{Na}^+$  (0.095 nm), the higher  $\text{K}^+$  concentration in the solution leads to a larger distance of the crystal plane for the particles obtained, and as a result, the KNN peaks gradually shifted to  $\text{KNbO}_3$  as clearly shown in the local enlarged XRD of Figure 10. The lattice parameters of the KNN particles were determined from the XRD data; the results are shown in Table 2.

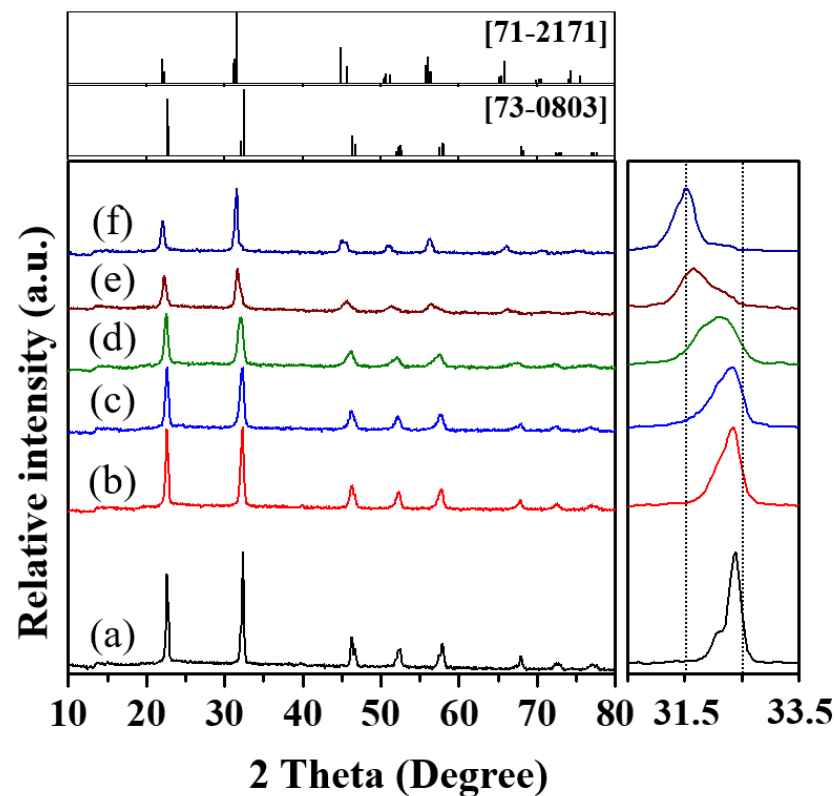


**Figure 10.** XRD patterns of KNN particles synthesized in glyothermal conditions with various molar ratios of  $K^+/Na^+$  at 200 °C for 12 h: (a) 1.0/1.0, (b) 1.4/0.6, (c) 1.5/0.5, (d) 1.6/0.4, (e) 1.7/0.3, and (f) 1.8/0.2. JCPDS database for  $KNbO_3$  (JCPDS card 71-2171) and  $NaNbO_3$  (JCPDS card 73-0803) are also included in the figure.

**Table 2.** The lattice parameters of KNN particles synthesized by glyothermal treatment with various molar ratios of  $K^+/Na^+$  at 200 °C for 12 h.

Molar Ratio ( $K^+/Na^+$ )	Lattice Parameters			Structure
	a (nm)	b (nm)	c (nm)	
1.0/1.0	0.5539	0.5576	1.5595	Orthorhombic
1.4/0.6	0.5557	0.5567	1.5609	Orthorhombic
1.5/0.5	0.5573	0.5576	1.5704	Orthorhombic
1.6/0.4	0.5567	0.3931	0.5618	Orthorhombic and Monoclinic [45]
1.7/0.3	0.5646	0.3933	0.5679	Orthorhombic
1.8/0.2	0.5713	0.3996	0.5740	Orthorhombic

When the molar ratio of  $K^+/Na^+$  was increased from 1.0/1.0 to 1.6/0.4, the XRD patterns of the obtained particles were the same as that of  $NaNbO_3$  (JCPDS card 73-0803), other than shifting a little to the left due to  $K^+$  dissolved into the  $NaNbO_3$  crystal. In the molar ratio of  $K^+/Na^+$  to 1.8/0.2 with a larger  $K^+$  concentration, the XRD patterns of the obtained particles are similar to that of  $KNbO_3$  (JCPDS card 71-2171). This result showed that the XRD patterns of  $KNbO_3$ -based single particles had shifted slightly to the right due to the  $Na^+$  dissolved into the  $KNbO_3$  crystal lattice. When the molar ratio of  $K^+/Na^+$  is in the experimentally optimized condition of 1.7/0.3, the  $K_{0.5}Na_{0.5}NbO_3$  particle at MPB composition could be synthesized by glyothermal conditions. The results were probably caused by the faster reaction between sodium and niobium in comparison with the one between potassium and niobium attributed to the different diffusivity of sodium ions and potassium ions, as previously reported [33,46–48]. In addition, Gibbs-free energy for  $NaNbO_3$  (−59 J/mol) is more negative than that of the  $KNbO_3$  (−49 J/mol) [49]. Because of

this result, the crystal distortion became more severe, and the crystal structure became more unstable. It could be assumed that the KNN form according to the following procedure:

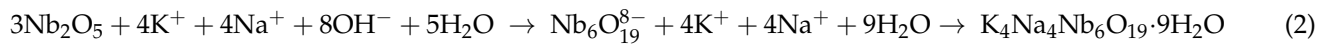
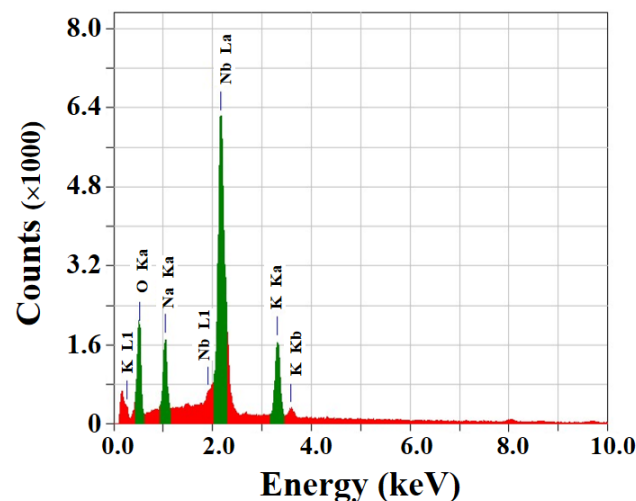


Figure 11 shows the EDS analysis results for KNN particles obtained at the glycothermal condition with different molar ratios of  $\text{K}^+/\text{Na}^+$ . The EDS spectra of all the particles obtained consisted of Na, K, Nb, and O elements attributed to the formation of KNN. However, the particle obtained in the molar ratio of  $\text{K}^+/\text{Na}^+$  to 1.0/1.0 was KNN particle lacking potassium, as shown in Figure 3b. Furthermore, the x value in the KNN particle was gradually increased with the increasing  $\text{K}^+$  concentration in the molar ratio of  $\text{K}^+/\text{Na}^+$ . The  $\text{K}_{0.5}\text{Na}_{0.5}\text{NbO}_3$  particle, which was MPB composition, could be synthesized by glycothermal condition at molar ratio of  $\text{K}^+/\text{Na}^+$  to 1.7/0.3 as shown in the EDS result of Figure 11. The particles obtained until the molar ratio of  $\text{K}^+/\text{Na}^+$  reached 1.6/0.4 have formed Na-rich KNN phase. When the molar ratio of  $\text{K}^+/\text{Na}^+$  is 1.8/0.2, the particles could obtain K-rich KNN phase with  $\text{K}^+$  content of approximately 72 mol%. The EDS analysis results for the changing  $\text{K}^+$  concentration in the KNN particles are quite similar to our XRD results. The calculated EDS results of each  $\text{K}^+$  content of KNN particles obtained at varying molar ratios of  $\text{K}^+/\text{Na}^+$  were presented in Table 3.



**Figure 11.** EDS analysis of KNN particles synthesized in glycothermal conditions with molar ratio of  $\text{K}^+/\text{Na}^+$  to 1.7/0.3 at 200 °C for 12 h.

**Table 3.** The calculated EDS results of each  $\text{K}^+$  content of KNN particles obtained in glycothermal conditions with varying molar ratios of  $\text{K}^+/\text{Na}^+$  at 200 °C for 12 h.

Samples (KOH/NaOH/Nb <sub>2</sub> O <sub>5</sub> )	1.0/1.0/0.1	1.4/0.6/0.1	1.5/0.5/0.1	1.6/0.4/0.1	1.7/0.3/0.1	1.8/0.2/0.1
Mole Content of $\text{K}^+$ (%) *	1	6	15	26	50	72
Phase		Na-rich KNN			MPB	K-rich KNN

\* An element of interest may be present below the detection limit of EDS (typically about 0.2–0.5%).

Figure 12 shows FE-SEM images of KNN particles glycothermally synthesized on the different molar ratios of  $\text{K}^+/\text{Na}^+$ . This result shows that the particles obtained at different molar ratios of  $\text{K}^+/\text{Na}^+$  were formed without a change of size and shape. The particles obtained under all conditions tended to have similar particle sizes and morphologies. All particles of hexahedron shape are aggregated with a relatively smaller primary

particle. The size and morphology of  $K_{0.5}Na_{0.5}NbO_3$  particles appeared as a hexahedron of approximately 400 nm.

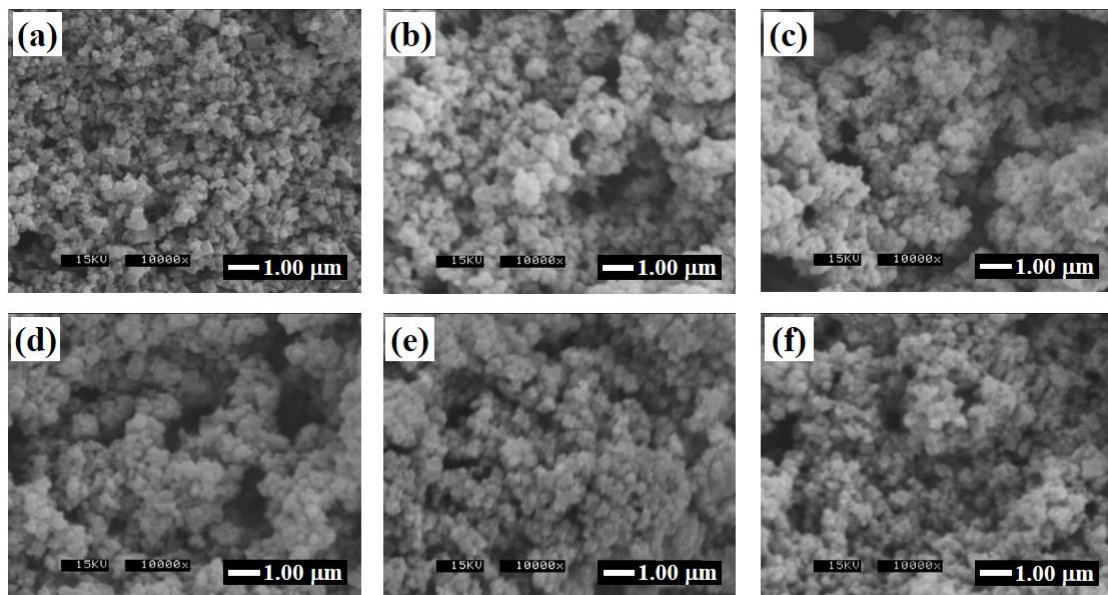


**Figure 12.** FE-SEM photographs of KNN particles synthesized in glycothermal conditions with various molar ratios of  $K^+/Na^+$  at 200 °C for 12 h: (a) 1.0/1.0, (b) 1.4/0.6, (c) 1.5/0.5, (d) 1.6/0.4, (e) 1.7/0.3, and (f) 1.8/0.2.

In addition, the particle size distributions of KNN particles synthesized with varying molar ratios of  $K^+/Na^+$  are shown in Figure 13. It could easily be seen from the results that the size distribution of all particles showed a similar tendency. The equivalent volume diameter of the Na-rich KNN particles was approximately 420 nm (Figure 13a,b), while that of the K-rich KNN particles was slightly decreased to 370 nm (Figure 13c).

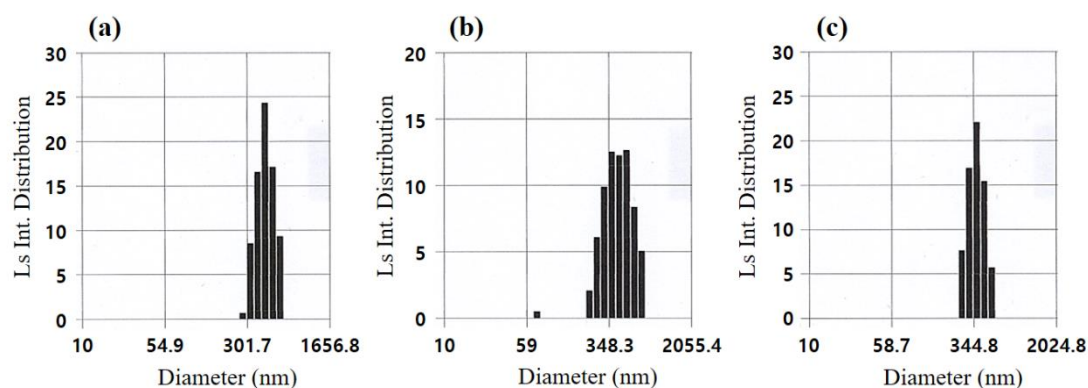


**Figure 13.** Particle size distribution of KNN particles synthesized in glycothermal conditions with various molar ratios of  $K^+/Na^+$  at 200 °C for 12 h: (a) 1.4/0.6, (b) 1.6/0.4, and (c) 1.8/0.2.

Figure 14 shows the TEM images and selected-area electron diffraction (SAED) pattern of the  $K_{0.5}Na_{0.5}NbO_3$  single crystal synthesized in glycothermal conditions with a molar ratio of  $K^+/Na^+$  to 1.7/0.3. The  $K_{0.5}Na_{0.5}NbO_3$  of the hexahedron shapes exhibits a single crystalline nature well dispersed with a sub-micron size of 300 nm, as shown in Figure 14a. The corresponding SAED pattern can be represented as orthorhombic phase of  $K_{0.5}Na_{0.5}NbO_3$  along the [001] zone axis, as shown in Figure 14b. The high-resolution TEM image also clearly reveals that the  $K_{0.5}Na_{0.5}NbO_3$  single crystals obtained exhibited lattice fringes with an inter-planar spacing of approximately 0.282 nm and 0.395 nm,

corresponding to the (200) and (010) plane of the orthorhombic structure, respectively, as shown in Figure 14c. These results are very consistent with that estimated by the XRD results.

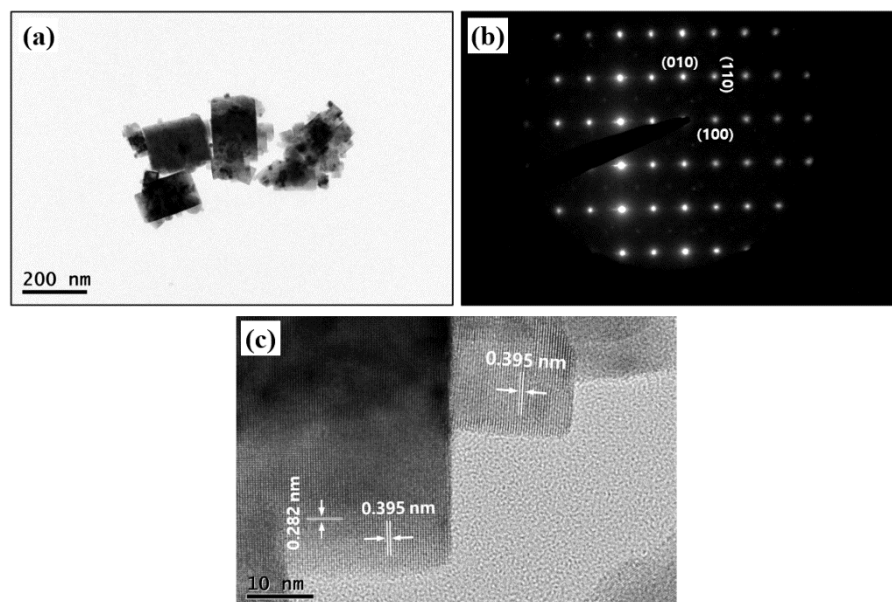


**Figure 14.** (a) TEM image, (b) SAED pattern, and (c) HRTEM image of  $K_{0.5}Na_{0.5}NbO_3$  particle of the MPB composition synthesized in glycothermal conditions at 200 °C for 12 h.

#### 4. Conclusions

Under the condition of molar ratio  $[1.0 + 1.0]/0.1$  of  $[K^+ + Na^+]/Nb$ , the phase pure KNN particles of perovskite-type structure without any impurities have been synthesized by a facile glycothermal method using 1,4-butanediol solvent at 200 °C for 12 h. It is considered that KNN was synthesized due to the increasing solubility of  $Nb_2O_5$  in the 1,4-butanediol solvent in which a strong base component was present with the increased reaction temperature and time. The obtained particles of hexahedron shapes are well dispersed with a relatively narrow particle size distribution and a size of 400 nm under glycothermal conditions. The particle size of KNN particles synthesized by the glycothermal method can be controlled from 15  $\mu m$  to 400 nm by adjusting the B/W solvent volume ratio from 0/70 to 70/0. The volume ratio of B/W in the reaction has a strong effect on the size of the synthesized KNN particles. It is considered that the nucleation and growth of KNN particles changed the in situ transition mechanism and dissolution-recrystallization by the reaction solvent, respectively. KNN particles with various potassium content of  $x$  value could be glycothermally synthesized by varying the molar ratios of  $K^+/Na^+$  in the fixed amount of  $Nb_2O_5$  (0.1 M). The  $K_{0.5}Na_{0.5}NbO_3$  particles of MPB composition with a size of approximately 400 nm and a hexahedron shape could be successfully synthesized by a glycothermal method on  $[K^+ + Na^+]/Nb$  molar ratio of  $[1.7 + 0.3]/0.1$  at 200 °C for 12 h. The glycothermal method has been confirmed to be a more efficient method for controlling the particle size of KNN particles from micro- to sub-micron.

**Author Contributions:** Conceptualization, H.-C.C., D.-Y.L. and J.-H.S.; data treatment and validation, H.-C.C., D.-Y.L. and J.-H.S.; investigation, H.-C.C., D.-Y.L. and J.-H.S.; visualization, H.-C.C. and J.-H.S.; writing—original draft resources, H.-C.C. and J.-H.S.; writing—review and editing, H.-C.C., D.-Y.L. and J.-H.S.; funding acquisition, J.-H.S. All authors have read and agreed to the published version of the manuscript.

**Funding:** This work was supported by a research grant from the PaiChai University in 2020 (No. 2020A0130).

**Institutional Review Board Statement:** Not applicable.

**Informed Consent Statement:** Not applicable.

**Data Availability Statement:** Not applicable.

**Conflicts of Interest:** The authors declare no conflict of interest.

## References

1. Jaffe, B.; Cook, W.R.; Jaffe, H. *Piezoelectric Ceramics*; Academic Press: New York, NY, USA, 1971; pp. 271–280.
2. Lu, Y.; Jeong, D.Y.; Cheng, Z.Y.; Zhang, Q.M.; Luo, H.S.; Yin, Z.W.; Viehland, D. Phase Transitional Behavior and Piezoelectric Properties of the Orthorhombic Phase of  $\text{Pb}(\text{Mg}_{1/3}\text{Nb}_{2/3})\text{O}_3$ - $\text{PbTiO}_3$  Single Crystals. *Appl. Phys. Lett.* **2001**, *78*, 3109–3111. [[CrossRef](#)]
3. Ren, W.; Liu, S.F.; Mukherjee, B.K. Piezoelectric Properties and Phase Transitions of  $\langle 001 \rangle$ -Oriented  $\text{Pb}(\text{Zn}_{1/3}\text{Nb}_{2/3})\text{O}_3$ - $\text{PbTiO}_3$  Single Crystals. *Appl. Phys. Lett.* **2002**, *80*, 3174–3176. [[CrossRef](#)]
4. Park, S.E.; Shrout, T.R. Ultrahigh Strain and Piezoelectric Behavior in Relaxor Based Ferroelectric Single Crystals. *J. Appl. Phys.* **1997**, *82*, 1804–1811. [[CrossRef](#)]
5. Guo, R.; Cross, L.E.; Park, S.E.; Noheda, B.; Cox, D.E.; Shirane, G. Origin of the High Piezoelectric Response in  $\text{PbZr}_{1-x}\text{Ti}_x\text{O}_3$ . *Phys. Rev. Lett.* **2000**, *84*, 5423–5426. [[CrossRef](#)]
6. Zheng, T.; Wu, J.; Xiao, D.; Zhu, J. Recent Development in Lead-Free Perovskite Piezoelectric Bulk Materials. *Progress Mater. Sci.* **2018**, *98*, 552–624. [[CrossRef](#)]
7. Panda, P.K. Review: Environmental friendly lead-free piezoelectric materials. *J. Mater. Sci.* **2009**, *44*, 5049–5062. [[CrossRef](#)]
8. Kosec, M.; Malič, B.; Benčan, A.; Rojac, T. KNN-Based Piezoelectric Ceramics. In *Piezoelectric and Acoustic Materials for Transducer Applications*; Safari, A., Akdoğan, E.K., Eds.; Springer: New York, NY, USA, 2008; pp. 81–102.
9. Zuo, R.; Rödel, J.; Chen, R.; Li, L. Sintering and Electrical Properties of Lead-Free  $\text{Na}_{0.5}\text{K}_{0.5}\text{NbO}_3$  Piezoelectric Ceramics. *J. Am. Ceram. Soc.* **2006**, *89*, 2010–2015. [[CrossRef](#)]
10. Lv, J.H.; Zhang, M.; Guo, M.; Li, W.C.; Wang, X.D. Hydrothermal Synthesis and Characterization of  $\text{K}_x\text{Na}_{(1-x)}\text{NbO}_3$  Powders. *Int. J. Appl. Ceram. Technol.* **2007**, *4*, 571–577. [[CrossRef](#)]
11. Wu, J.; Xiao, D.; Zhu, J. Potassium–Sodium Niobate Lead-Free Piezoelectric Materials: Past, Present, and Future of Phase Boundaries. *Chem. Rev.* **2015**, *115*, 2559–2595. [[CrossRef](#)]
12. Lin, D.; Kwok, K.W.; Chan, H.L.W. Phase transition and electrical properties of  $(\text{K}_{0.5}\text{Na}_{0.5})(\text{Nb}_{1-x}\text{Ta}_x)\text{O}_3$  lead-free piezoelectric ceramics. *Appl. Phys. A-Mater. Sci. Process.* **2008**, *91*, 167–171. [[CrossRef](#)]
13. Yang, S.L.; Tsai, C.C.; Hong, C.S.; Chu, S.Y. Effects of sintering aid  $\text{CuTa}_2\text{O}_6$  on piezoelectric and dielectric properties of sodium potassium niobate ceramics. *Mater. Res. Bull.* **2012**, *47*, 998–1003. [[CrossRef](#)]
14. Kupec, A.; Malic, B.; Tellier, J.; Tchernychova, E.; Glinsek, S.; Kosec, M. Lead-Free Ferroelectric Potassium Sodium Niobate Thin Films from Solution: Composition and Structure. *J. Am. Ceram. Soc.* **2012**, *95*, 515–523. [[CrossRef](#)]
15. Li, J.F.; Wang, K.; Zhu, F.Y.; Cheng, L.Q.; Yao, F.Z. (K, Na) $\text{NbO}_3$ -Based Lead-Free Piezoceramics: Fundamental Aspects, Processing Technologies, and Remaining Challenges. *J. Am. Ceram. Soc.* **2013**, *96*, 3677–3696. [[CrossRef](#)]
16. López-Juárez, R.; González, F.; Villafuerte-Castrejón, M.E. Lead-free ferroelectric ceramics with perovskite structure. *Ferroelectr. Mater. Aspects.* **2011**, *5*, 305–330.
17. Gu, H.; Zhu, K.; Pang, X.; Shao, B.; Qiu, J.; Ji, H. Synthesis of (K, Na) (Nb, Ta) $\text{O}_3$  lead-free piezoelectric ceramic powders by high temperature mixing method under hydrothermal conditions. *Ceram. Int.* **2012**, *38*, 1807–1813. [[CrossRef](#)]
18. Park, S.H.; Ahn, C.W.; Nahm, S.; Song, J.S. Microstructure and Piezoelectric Properties of ZnO-added  $(\text{Na}_{0.5}\text{K}_{0.5})\text{NbO}_3$  Ceramics. *Jpn. J. Appl. Phys.* **2004**, *43*, L1072–L1074. [[CrossRef](#)]
19. Lim, J.B.; Zhang, S.; Jeon, J.-H.; Shrout, T.R. (K,Na) $\text{NbO}_3$ -based ceramics for piezoelectric hard lead-free material. *J. Am. Ceram. Soc.* **2010**, *93*, 1218–1220. [[CrossRef](#)]
20. Zeng, J.T.; Kwok, K.W.; Chan, H.L.W.  $\text{K}_x\text{Na}_{1-x}\text{NbO}_3$  powder synthesized by molten-salt process. *Mater. Lett.* **2007**, *61*, 409–411. [[CrossRef](#)]
21. López-Juárez, R.; Castañeda-Guzmán, R.; Rubio-Marcos, F.; Villafuerte-Castrejón, M.E.; Barrera-Calvad, E.; González, F. Insights into the dielectric and luminescent properties of  $\text{Na}_{0.5}\text{Pr}_{0.003}\text{Bi}_{0.497-x}\text{La}_x\text{TiO}_3$  synthesized by the Pechini method. *Dalton Trans.* **2013**, *42*, 6879–6885. [[CrossRef](#)]
22. Hussain, F.; Khesro, A.; Muhammad, R.; Wang, D. Effect of Ta-doping on functional properties of  $\text{K}_{0.51}\text{Na}_{0.49}\text{NbO}_3$ . *Mater. Res. Express* **2019**, *6*, 106309. [[CrossRef](#)]
23. Malic, B.; Bernard, J.; Holc, J.; Jenko, D.; Kosec, M. Alkaline-earth doping in (K,Na) $\text{NbO}_3$  based piezoceramics. *J. Eur. Ceram. Soc.* **2005**, *25*, 2707–2711. [[CrossRef](#)]
24. Ribeiro, C.A.; Eiras, J.A.; Lente, M.H. Sintering kinetics of  $(\text{K}_{0.48}\text{Na}_{0.52})\text{NbO}_3$  lead-free piezoelectric ceramics densified by spark plasma sintering: Construction of master sintering curve. *Ferroelectrics* **2019**, *545*, 80–88. [[CrossRef](#)]
25. Li, X.; Fan, B.; Lu, H.; Wang, H.; Shao, G.; Zhang, R. Investigation on preparation of  $\text{Na}_{0.5}\text{K}_{0.5}\text{NbO}_3$  nanoparticles by microwave heating method. *Mater. Res. Express* **2018**, *5*, 115018. [[CrossRef](#)]
26. Khorrani, G.H.; Kompany, A.; Zak, A.K. Structural and optical properties of (K,Na) $\text{NbO}_3$  nanoparticles synthesized by a modified sol-gel method using starch media. *Adv. Powder Technol.* **2015**, *26*, 113–118. [[CrossRef](#)]

27. Wang, H.; Zuo, R.; Fu, J.; Liu, Y. Sol-gel derived (Li, Ta, Sb) modified sodium potassium niobate ceramics: Processing and piezoelectric properties. *J. Alloy. Compd.* **2011**, *509*, 936–941. [[CrossRef](#)]
28. Zhang, D.-Q.; Qin, Z.C.; Yang, X.Y.; Zhu, H.B.; Cao, M.S. Study on synthesis and evolution of sodium potassium niobate ceramic powders by an oxalic acid-based sol-gel method. *J. Sol-Gel Sci. Technol.* **2011**, *57*, 31–35. [[CrossRef](#)]
29. Sun, C.; Xing, X.; Chen, J.; Deng, J.; Li, L.; Yu, R.; Qiao, L.; Liu, G. Hydrothermal Synthesis of Single Crystalline (K,Na)NbO<sub>3</sub> Powders. *Eur. J. Inorg. Chem.* **2007**, *13*, 1884–1888. [[CrossRef](#)]
30. Piskin, C.; Karacasulu, L.; Bortolotti, M.; Vakifahmetoglu, C. Synthesis of potassium–sodium niobate (KNN) from NbO<sub>2</sub>. *Open Ceram.* **2021**, *7*, 100159. [[CrossRef](#)]
31. Skjærø, S.L.; Wells, K.H.; Beek, W.; Grande, T.; Einarsrud, M.A. Kinetics of the hydrothermal synthesis of nanosized K<sub>x</sub>Na<sub>1-x</sub>NbO<sub>3</sub>. *CrystEngComm* **2018**, *20*, 6795–6802. [[CrossRef](#)]
32. Shi, G.; Wang, J.; Wang, H.; Wu, Z.; Wu, H. Hydrothermal synthesis of morphology-controlled KNbO<sub>3</sub>, NaNbO<sub>3</sub>, and (K,Na)NbO<sub>3</sub> powders. *Ceram. Int.* **2017**, *43*, 7222–7230.
33. Zhang, F.; Han, L.; Bai, S.; Sun, T.; Karaki, T.; Adachi, M. Hydrothermal synthesis of (K,Na)NbO<sub>3</sub> particles. *Jpn. J. Appl. Phys.* **2008**, *47*, 7685–7688. [[CrossRef](#)]
34. Ramajo, L.A.; Rubio-Marcos, F.; Campo, A.D.; Fernández, J.F.; Castro, M.S.; Parra, R. New insights into the properties of K<sub>x</sub>Na<sub>(1-x)</sub>NbO<sub>3</sub> ceramics obtained by hydrothermal synthesis. *Ceram. Int.* **2014**, *40*, 14701–14712. [[CrossRef](#)]
35. Kim, B.K.; Lim, D.Y.; Riman, R.E.; Nho, J.S.; Cho, S.B. A New Glycothermal Process for Barium Titanate Nanoparticle Synthesis. *J. Am. Ceram. Soc.* **2003**, *86*, 1793–1796. [[CrossRef](#)]
36. Jung, Y.J.; Lim, D.Y.; Nho, J.S.; Cho, S.B.; Riman, R.E.; Lee, B.W. Glycothermal synthesis and characterization of tetragonal barium titanate. *J. Cryst. Growth* **2005**, *274*, 638–652. [[CrossRef](#)]
37. Cho, S.B.; Noh, J.S.; Park, S.J.; Lim, D.Y.; Choi, S.H. Morphological control of Fe<sub>3</sub>O<sub>4</sub> particles via glycothermal process. *J. Mater. Sci.* **2007**, *42*, 4877–4886.
38. Ryu, J.H.; Kil, H.S.; Song, J.H.; Lim, D.Y.; Cho, S.B. Glycothermal synthesis of 3 mol% yttria stabilized tetragonal ZrO<sub>2</sub> nano powders at low temperature without mineralizers. *Powder Technol.* **2012**, *221*, 228–235. [[CrossRef](#)]
39. Kil, H.S.; Jung, Y.J.; Moon, J.I.; Song, J.H.; Lim, D.Y.; Cho, S.B. Glycothermal Synthesis and Photocatalytic Properties of Highly Crystallized Anatase TiO<sub>2</sub> Nanoparticles. *J. Nanosci. Nanotechnol.* **2015**, *15*, 6193–6200. [[CrossRef](#)]
40. Ryu, J.H.; Kongsy, P.; Lim, D.Y.; Cho, S.B.; Song, J.H. Facile glycothermal synthesis of ZnO nanopowder at low temperature. *Ceram. Int.* **2016**, *42*, 17565–17570. [[CrossRef](#)]
41. Park, S.J.; Song, J.H. Glycothermally Synthesized Self-aggregated ZnS Spherical Particles for Methyl Orange Photodecomposition. *Korean J. Met. Mater.* **2021**, *59*, 732–740. [[CrossRef](#)]
42. Deblonde, G.J.-P.; Chagnes, A.; Bélaïr, S.; Cote, G. Solubility of niobium(V) and tantalum(V) under mild alkaline conditions. *Hydrometallurgy* **2015**, *156*, 99–106. [[CrossRef](#)]
43. Mullin, J.W. Crystal growth in pure and impure systems. In *Industrial Crystallization 78*; de Jong, E.J., Jancic, S.J., Eds.; North Holland: Amsterdam, The Netherlands, 1979; pp. 93–103.
44. Randolph, A.D.; Larson, M.A. *Theory of Particulate Processes: Analysis and Techniques of Continuous Crystallization*, 2nd ed.; Academic Press, Inc.: San Diego, CA, USA, 1988; pp. 109–134.
45. Baker, D.W.; Thomas, P.A.; Zhang, N.; Glazer, A.M. Structural study of K<sub>x</sub>Na<sub>1-x</sub>NbO<sub>3</sub> (KNN) for compositions in the range  $x = 0.24$ – $0.36$ . *Acta Cryst. B* **2009**, *65*, 22–28. [[CrossRef](#)] [[PubMed](#)]
46. Park, S.; Peddigari, M.; Kim, J.H.; Kim, E.; Hwang, G.-T.; Kim, J.-W.; Ahn, C.-W.; Choi, J.-J.; Hahn, B.-D.; Choi, J.-H.; et al. Selective phase control of dopant-free potassium sodium niobate perovskites in solution. *Inorg. Chem.* **2020**, *59*, 3042–3052. [[CrossRef](#)]
47. Lin, T.-H.; Yund, R. Potassium and sodium self-diffusion in alkali feldspar. *Contrib. Mineral. Petrol.* **1972**, *34*, 177–184. [[CrossRef](#)]
48. Malic, B.; Jenko, D.; Holc, J.; Hrovat, M.; Kosec, M. Synthesis of sodium potassium niobate: A diffusion couples study. *J. Am. Ceram. Soc.* **2008**, *91*, 1916–1922. [[CrossRef](#)]
49. Zhang, C.; LV, H.; Guo, M.; Zhang, M.; Wang, X. Thermodynamic evaluation and hydrothermal preparation of K<sub>x</sub>Na<sub>1-x</sub>NbO<sub>3</sub>. *Rare Metals* **2008**, *27*, 371–377. [[CrossRef](#)]